

# A NEW APPLICATION FOR 3D-SNAKES

## *Modelling Electrical Discharges*

Gilmario Barbosa dos Santos

*University of State of Santa Catarina, UDESC-DCC, Joinville-SC, Brazil*

Sidney Pinto da Cunha

*Center of Information Technology Renato Archer, CTI-DRVC, Campinas-SP, Brazil*

Clesio Luiz Tozzi

*University of Campinas, UNICAMP-FEEC-DCA, Campinas-SP, Brazil*

**Keywords:** B-spline, Snakes, 3D image reconstruction, Camera calibration, Electrical discharges characterization.

**Abstract:** A new approach for modelling electrical discharges is proposed. To this purpose, an active contour named *3D-snake* is used that is geometrically represented by a *B-spline* which evolves in 3D space constrained by internal and external energies. More specifically, this external energy come from a pair of images. This new model is much less dependent on determination of homologous points than the approaches found in the literature for recovering 3D geometry of electrical discharges. In addition, the proposal discussed here is capable of tracking the evolution of the electrical discharge taking into account the time dependence between consecutive pairs of frames in two videos.

## 1 INTRODUCTION

Computer vision techniques have applied stereopsis in images of electrical discharges. Some works as MacAlpine and Qiu (MacAlpine et al., 1999), Qiu et al. (Qiu and MacAlpine, 2000; Qiu et al., 1999) and Amarasinghe et al. (Amarasinghe et al., 2007) present some important results in this field but their strategies are strongly dependent on explicit methods of homologous determination, and furthermore these methods are applied for electrical discharges with low level of curvature and wavy discharges are avoided in their experiments. On the other hand, here we propose a new approach based on 3D snakes for modelling the longitudinal medial-axes of electrical discharges based on two digital videos which practically makes correspondences determination unnecessary.

In the bi-dimensional case ((Kass et al., 1988)), the snakes are modelled by a energy functional that is minimized under certain constraints, as a consequence the snake deforms itself looking for some feature of interest in the image. The 3D snake is a model

based on the same principles, which means that the 3D snake also has a functional of energy with geometric and photometric constraints. The aspect that differentiates 3D snake is related to its external energy which is extracted from more than one image, which means that the external energy must come from 2D spaces determining a 3D force, i.e., the external energy emerges from a stereo pair of images.

Although very commonly applied in solving the functional in bi-dimensional snakes, neither Dynamic Programming (Amini et al., 1988) nor Greedy Algorithms (Williams and Shah, 1992) are useful in the case of 3D snakes. The approach here is based on Cañero (Canero et al., 2000; Canero, 2002) which does not explore the methods based on meta heuristic.

In the stereopsis of two digital videos, the key aspect in recovering a 3D global/world point from images, is the identification of homologous points in the images. Finding homologous points is a hard problem in stereopsis, although correlation is usually applied for this sake but sometimes does not succeed. Consid-

ering a sequence (or video) of stereo pairs of electrical discharge, the 3D-snake approach practically dispense the homologous determination.

The methodology for validating the approach described here is based on a set of images built by the simulation of an image acquisition system that captures a mathematical curve in evolution in 3D space. After validation the method was applied on electrical arcs stereo pairs.

In the next section (2) will be described the precursor snake model and a the 3D snake model (3). Following a description of the experiment development is given and the results reported (section 4). Finally, the approach is applied on images of electrical discharges.

## 2 THE PRECURSOR SNAKE MODEL

The model of snakes was first proposed by Kass et al. (Kass et al., 1988), it is a physical inspired model based on the functional of energy below.

$$E_{total} = \int_0^1 E_{int}(v(s)) + E_{ext}(v(s))ds. \quad (1)$$

In the Eq. (1), the snake is the contour  $v(s)$  and coordinates  $x$  and  $y$  are determined by the parameter  $s$ , so  $v(s) = (x(s), y(s))$ , and the precursor snake can be seen as defined in a bi-dimensional cartesian space. The external energy  $E_{ext}(v(s))$  represents the photometric constraint originated from the image and should be defined conveniently in order to generate the force to guide the snake to the object of interest in the image. In turn, the internal energy  $E_{int}(v(s))$  is the geometric constraint representing the smoothness grade (first and second order of continuity) of the active contour. This aspect can be distinguished by checking the definition of the internal energy. Note that, according to Eq. (2) below, the terms  $\frac{\partial v(s)}{\partial s}$  and  $\frac{\partial^2 v(s)}{\partial s^2}$  determine the first and second order continuity, respectively. Also observe that the forces originated by internal energy are intrinsic characteristics of the snake.

In Eq.(2), the parameters  $\alpha$  and  $\beta$  weigh the terms in order to control the geometry of the contour defining how much of it could be wavy or not.

$$E_{int}(v(s)) = \frac{1}{2} \int_0^1 \left( \alpha(s) * \left| \frac{\partial v(s)}{\partial s} \right|^2 + \beta(s) * \left| \frac{\partial^2 v(s)}{\partial s^2} \right|^2 \right) d(s). \quad (2)$$

In terms of numerical methods the functional is solved by the relaxation according to equations (3) and (4) below (Kass et al., 1988), where  $\alpha$  and  $\beta$  are

introduced in the pentadiagonal matrix  $A$ , described in (Ihlow and Seiffert, 2005) and (Kass et al., 1988), called stiffness matrix. The  $\gamma$  parameter is used for weighing the external forces.

$$x_t = (A + \gamma I)^{-1}(x_{t-1} - F_x) \quad (3)$$

$$y_t = (A + \gamma I)^{-1}(y_{t-1} - F_y) \quad (4)$$

In fact, Eq. (3) and Eq. (4) can be compressed into Eq. (5), where  $v_t = (x_t, y_t)$  is a point of the snake in bi-dimensional space and  $F$  corresponds to the external force composed by  $F_x, F_y$ .

$$v_t = (A + \gamma I)^{-1}(v_{t-1} - F) \quad (5)$$

Although has been initially proposed in 1988 the active contours is still alive as can be seen in recent works such as (Thevenaz and Unser, 2008).

## 3 3D-SNAKE

The 3D-snake is similar to the 2D precursory model described above but the functional has external energies defined in 3D space and the external forces act upon the control points of a B-spline which represents the 3D-snake geometrically.

The 3D-snake corresponds to a B-spline which deforms itself in 3D space in order to match its projections with a pair of features of interest in two images. As mentioned before, the external force is recovered from a pair of images (in fact a pair of vectorial maps) through triangulation, see Trucco and Verri (Trucco and Verri, 1998) or another stereo vision method. It is important to note that for 3D-snakes the external force does come from the same dimensional space of the snake itself. This aspect is an important difference to the prior snake model proposed by Kass et al. (Kass et al., 1988). Since, in that case the snake evolved in the same bi-dimensional space from where the external forces were extracted.

The 3D-snakes implemented here were inspired mainly in the works of Cañero (Canero et al., 2000; Canero, 2002).

### 3.1 Initialization

Cañero in (Canero et al., 2000; Canero, 2002) describes a manual determination of homologous from which a set of 3D points are recovered for initialization of the first 3D-snake. In the proposal described here, the initialization almost dispense homologous determination and consists of automatic procedure. This initialization will be described in details later on. The next paragraphs are focused in describing the

steps needed to get the first 3D-snake after determination of the initial 3D points.

The inaccurate set of 3D points is approximated (not interpolated) by a third order piecewise polynomial B-spline which will represent the 3D-snake. An interpolation would force the B-spline to go through all of the 3D data points which is not convenient because the B-spline resultant will be very wavy. So, the best choice is doing an approximation in order to obtain a smooth B-spline which does not necessarily pass through every 3D data points; Rogers and Adams (Rogers and Adams, 1990) provides practical methods in order to solve this problem.

The functional of energy associated is defined and the 3D-snake deforms by minimization of this functional under geometrical and photometrical constraints. This minimization process leads the control points of the B-spline in order to guide the projections of the points generated by the B-spline (3D-snake) in the direction of the features of interest in the pair of images. When the projections match the features that have been pointed out, the best configuration of the 3D-snake will have been reached and consequently the best 3D spatial location of the longilineous object represented by the snake.

For a clearer understanding, consider a pair of videos with  $k$  pairs of frames obtained in time  $i \in 0, 1, \dots, k-1$ . The proposal is to adjust the 3D snake  $\mathcal{B}_i$ , to the pair of vectorial maps  $(m_{i+1}^1, m_{i+1}^2)$  representing external forces in time  $i+1$ . So, after time  $k-1$  all of the possible configuration of the 3D snake will be covered and consequently the object represented by the 3D-snake will be tracked. Since the cameras have been calibrated it is even possible to measure this object.

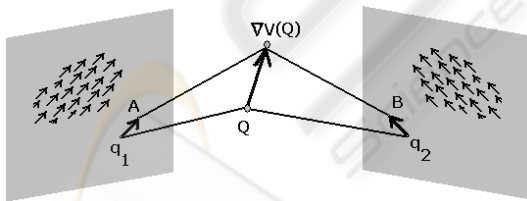


Figure 1: The external force is recovered from the space of vectorial maps. The resultant 3D vector acts over the nodes of the 3D-snake (in fact upon the control points of the B-spline that represents it) deforming it in order to adapt its own projections over a pair of images.

### 3.2 The Functional of Energy

The initialization gives the third order B-spline  $\mathcal{B}_0$ , it is customary to describe a B-spline by a matricial equation like in Eq. (6), where  $\mathbf{Q}$  represents a point generated by the B-spline through the set of control

points  $\mathbf{V}$  and the basis functions matrix  $\mathbf{N}$ . This matricial formulation will be used here.

$$\mathbf{Q} = \mathbf{N}\mathbf{V} \quad (6)$$

The deformation of the 3D snake is defined by a functional of energy which is very similar to the one presented in Eq. (1) but here the active contour is represented by a B-spline:

$$E(\mathbf{Q}) = \int E_{int}(\mathbf{Q}) + E_{ext}(\mathbf{Q}) ds. \quad (7)$$

Similarly to Kass et al. (Kass et al., 1988), the  $E_{int}$  preserves smoothness at the same time that  $E_{ext}$  is responsible for the forces which attract the 3D-snake, pushing into the features of interest captured in the images. Again, the minimization occurs by relaxation such as is defined in Eq. (8), which is similar to Eq. (5) except that here the minimization acts on the control points of the B-spline, so that a new set of control points  $\mathbf{V}_t$  is calculated based on the old set  $\mathbf{V}_{t-1}$ :

$$\mathbf{V}_t = (\mathbf{H} + \gamma\mathbf{I})^{-1}(\gamma\mathbf{V}_{t-1} - \mathbf{g}(\mathbf{Q}_{t-1})) \quad (8)$$

Moreover, other important aspects and some similarities between Eq. (8) and Eq. (5) must be emphasized, as follows:

- Note, the matrix  $\mathbf{H}$  corresponds to the stiffness matrix  $\mathbf{A}$  as seen in Eq. (5). The construction of  $\mathbf{H}$  will be discussed later.
- The vector  $\mathbf{g}(\mathbf{Q})$  corresponds to the external force transformed into the space of control points, therefore, the term  $\mathbf{V}_{t-1} - \mathbf{g}(\mathbf{Q})$  attracts the control points and consequently  $\mathbf{Q}(s)$  in the direction of the features of interest depicted in the images.

For calculating  $\mathbf{g}(\mathbf{Q})$  Cañero (Canero, 2002) recommends the approximation described in Eq. (9), where  $\mathbf{N}$  is the basis functions matrix used in Eq. (6):

$$\mathbf{g}(\mathbf{Q}) \approx \mathbf{N}^T F_{ext}(\mathbf{Q}) \quad (9)$$

- The external force  $F_{ext}$  is recovered from vectorial maps (from 2D to 3D space). As shown in Fig. 1, the homologous points  $\mathbf{q}_1$  and  $\mathbf{q}_2$  are associated to the vectors  $(\mathbf{A} - \mathbf{q}_1)$  and  $(\mathbf{B} - \mathbf{q}_2)$ , respectively in 2D space (vectorial maps), therefore a triangulation (as in Trucco and Verri (Trucco and Verri, 1998)) of the end points of these vectors (point A and B) gives the 3D force that acts upon a point in the B-spline. The set of all 3D forces calculated builds the vector  $F_{ext}$  which is transformed into the space of control points, giving birth to vector  $\mathbf{g}(\mathbf{Q})$  in Eq. (9).

By inspecting Fig. 1, geometrically the overall formula to get  $F_{ext}$  can be seen in Eq. (10), be-

low.

$$\begin{aligned} \mathbf{F}_{ext}(\mathbf{Q}) &= -\nabla\mathbf{V}(\mathbf{Q}) \Rightarrow \\ \mathbf{F}_{ext}(\mathbf{Q}) &= \varphi^{-1}(\mathbf{q}_1 - \nabla\mathbf{V}_1(\mathbf{q}_1), \mathbf{q}_2 - \nabla\mathbf{V}_2(\mathbf{q}_2)) - \mathbf{Q} \\ \varphi^{-1} &\text{ is the operator of triangulation} \end{aligned} \quad (10)$$

Finally,  $\mathbf{g}(\mathbf{Q})$  is substituted in Eq. (8), in the term  $(\mathbf{V}_{t-1} - \mathbf{g}(\mathbf{Q}))$  which plays the role of attracting the B-spline's control points to the features of interest in images. Since the B-spline represents the 3D-snake, pushing the first implies in guiding the second to the features of interest.

### 3.3 The Matrix $\mathbf{H}$

Similarly to matrix  $\mathbf{A}$  in Eq. (5), matrix  $\mathbf{H}$  represents the stiffness of the 3D snake model. The parameters  $\alpha$  and  $\beta$  are embedded in  $\mathbf{H}$ , so  $\mathbf{H}$  acts on the control points of the B-spline that represents the 3D-snake determining its flexibility. Cañero (Canero, 2002) suggests calculating  $\mathbf{H}$  according Eq. (11), below:

$$\mathbf{H} = \frac{1}{L} \sum_{\sigma=0}^{L-1} \mathbf{G}_{\sigma}^T \mathbf{N}_{\sigma}^S \mathbf{N}_{\sigma}^{S^T} (\alpha \mathbf{P}' + \beta \mathbf{P}'') \mathbf{N}_{\sigma}^S \mathbf{G}_{\sigma} \quad (11)$$

Note that:

- $L$ : the number of spans in the vector of knots of the B-spline;
- $\mathbf{N}_{\sigma}^S$ : the matrices of span, which could be calculated algorithmically, Blake and Isard (Blake and Isard, 2000) present such algorithm;
- $\mathbf{G}_{\sigma}$ : the matrices  $\mathbf{G}_{\sigma}$  present  $d \times N_B$  and are used to select one subset of control points consecutively. Differently than Blake and Isard (Blake and Isard, 2000) here the expression in Eq. (12) will be applied for defining  $\mathbf{G}_{\sigma}$ , as shown below:

$$(\mathbf{G}_{\sigma})_{ij} = \begin{cases} 1 & \text{if } j - b_{\sigma} = i; \\ 0 & \text{otherwise.} \end{cases} \quad (12)$$

Where:

$$b_{\sigma} = \left( \sum_{i=0}^{\sigma} m_i \right) - d \quad (13)$$

Note that:

- $\sigma$  corresponds to one span of the vector of knots of the B-spline;
- $m_i$  is the multiplicity of the  $i$ -th knot in the vector of knots;
- $d$  corresponds to the order of the B-spline.
- $\mathbf{P}'$  and  $\mathbf{P}''$  According to Cañero (Canero, 2002) the first and second derivatives of  $\mathbf{P}$  (a Hilbert matrix<sup>1</sup>) can be calculated by Eq. (14) and Eq.

<sup>1</sup>Hilbert Matrix  $H_{ij} = \int_0^1 a_{ij}^{i-1} b_{ij}^{j-1} dx$

(15). Such formulas differs from (Blake and Isard, 2000) but are more appropriate.

$$\mathbf{P}' = \begin{cases} 0 & \text{if } i = 1 \text{ or } j = 1; \\ \frac{(i-1)(j-1)}{i+j-3} & \text{otherwise} \end{cases} \quad (14)$$

$$\mathbf{P}'' = \begin{cases} 0 & \text{if } i < 3 \text{ or } j < 3 \\ \frac{(2-3i+i^2)(2-3j+j^2)}{i+j-5} & \text{otherwise} \end{cases} \quad (15)$$

## 4 VALIDATING THE PROPOSAL

A sequence of image pairs for testing the model were generated. The images were calculated according to mathematical function described in the next section which create an evolving curve in the 3D space. Provided such images, the 3D-snake should be initialized and forced to deform by the relaxation as described in Eq. (8) constrained by the external and internal forces. Being a model for the real curve, the 3D-snake should track it. The accuracy of this tracking can be easily evaluated because the real curve is known. The methodology for evaluation consists in measuring the length of each instance of the real curve ( $L_i$ ) for comparison with the lengths estimated by the 3d-snake model ( $L_i^{snake}$ ). Also, the deviation between real and estimated lengths is calculated. The curvature of each real curve is used to evaluate the robustness of the model for wavy instances of the curve.

Given a point  $p_j$  the curvature in this point can be approximated by the second derivative taking into account its two adjacent neighbors. Eq. (16) below is used for determination of the total curvature of the  $i$ -th configuration of the curve ( $Curv^i$ ):

$$Curv^i = \sum_{j=2}^{N-1} curv_j \quad (16)$$

Note:

$$curv_j = \| p_{j-1} - 2 * p_j + p_{j+1} \|^2 \quad (17)$$

The percentual deviation of each length measure of the  $i$ -th 3D-snake ( $L_i^{snake}$ ) is done by Eq. (18) as shown below:

$$d_i^{perc} = \frac{|L_i - L_i^{snake}|}{L_i} * 100 \quad (18)$$

### 4.1 Mathematical Curve

An image database was built from the curves according the Eq. (19) which describes the family of helices depicted in Fig. 2. Each pair of images results from

projections of the respective member of this family. Each helix member is determined by Eq. (19) using  $w_1(t) = \frac{t}{1000}$ ,  $w_2(t) = \frac{t}{100}$  and  $v = 4$ . The first curve is not exactly an helix but a straight line along the axis  $OY$  that smoothly transforms itself into an helix as an spring that is strongly stretched and then gradually released (Fig. 2).

For each incoming value of  $r_t$  and using the parameters of the cameras stipulated according to the geometry shown in Fig. 3 and Fig. 4 the respective spatial configuration of the curve is captured by the pair of virtual cameras.

$$C(t) = \begin{cases} \mathbf{x}(t) &= r_t * \sin(w_1(t) * \mathbf{a}); \\ \mathbf{y}(t) &= v * \mathbf{a}; \\ \mathbf{z}(t) &= r_t * \cos(w_2(t) * \mathbf{a}); \end{cases} \quad (19)$$

Notes:

- 1)  $\mathbf{a}$ ,  $\mathbf{x}$ ,  $\mathbf{y}$  and  $\mathbf{z}$  are vectors;
- 2)  $\mathbf{a} = (\theta_0, \theta_1, \dots, \theta_{max})$  in radians;
- 3)  $w_1(t)$  and  $w_2(t)$ : angular velocities;
- 4)  $v$ : velocity along axis  $OY$ ;
- 5)  $r_t$ : the discretely crescent ray of the helix,  $r_t \in \{t_0, t_1, \dots, t_j, \dots, t_{max}\}$ ,  $t_0 = 1$  and  $t_{j-1} < t_j < t_{j+1}$ .

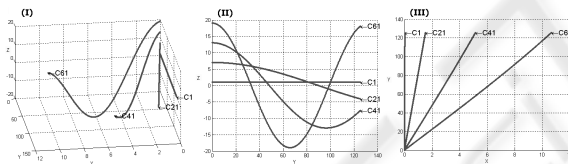


Figure 2: (I) Samples of the family of helices obtained by Eq. (19). (II) View of curves from ZY plane. (III) And view from XY plane.

## 4.2 Images Acquisition System

A sufficient number of points of the mathematical curve is generated and projected in the respective image plane of two virtual pinhole cameras (see Fig. 4). Both are defined by their respective extrinsic ( $\mathbf{R}$  and  $\mathbf{T}$ ) and intrinsic parameters (focal distance, dimensions of pixels, principal point). In terms of geometry, the extrinsic parameters describe the relation between the coordinates of a point in global/world  $\mathbf{P}_g$  and a point in the 3D camera system  $\mathbf{P}_c$ ; here we adopt the following relation  $\mathbf{P}_g = \mathbf{R}\mathbf{P}_c + \mathbf{T}$  and a geometry such as that shown in Fig. 3.

By repetition of this process, for various spatial configurations of the curve, two sets of frames were consistently created.

Considering the definition of intrinsic and extrinsic parameters for both virtual cameras it is possible

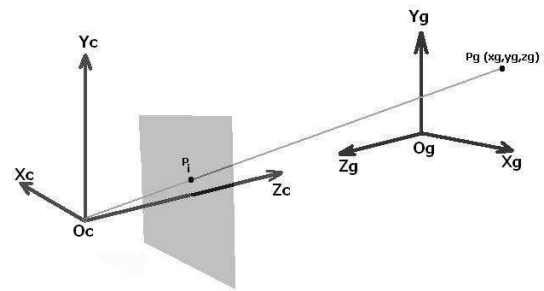


Figure 3: The geometry of a pinhole camera model with image plane in front of the principal point (focus) of the camera. Axis  $Ox_g$ ,  $Oy_g$  and  $Oz_g$  define the global/world coordinate system,  $Ox_c$ ,  $Oy_c$  and  $Oz_c$  refer to the camera system.

to project the points generated by the mathematical function in both image planes, and right cameras (see Fig. 4). By repetition of this process for various spatial configurations of the curve two sets of frames are captured.

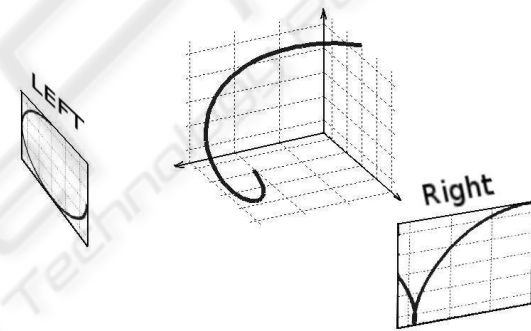


Figure 4: A curve in 3D space has its points projected in a pair of image planes left and right.

## 4.3 Vectorial Maps

Provided that the two sequences of frames (from the left and right cameras) were acquired, the next step is to transform them in vectorial maps for representing the external forces components.

Usually, image processing operations are done for emphasizing features of interest in each frame of the sequence. At the same time, to prepare the images to be transformed by a differential operator such as the gradient. In this work the distance transform is used in order to generate a matrix whose cells represents a pixel in the respective frame (image) and stores the distance from this pixel to the projection of the curve. Then, this map of distances is operated by the GVF (Xu and Prince, 1998) originating two matrices with the horizontal and vertical components of the gradient vectors. For the sake of simplicity, these two matrices will be considered as just one matrix of

resultant gradient vectors, which will be called as the vectorial map associated to its respective frame (image). These maps are responsible for the vectors  $q_1A$  and  $q_2B$  as shown in Fig. 1. Fig. 5 shows the result of transformation by distance transform and respective vectorial map.

Three views of the same distance map could be seen in Fig. 6, emphasizing its topological attributes with the feature of interest in the bottom of a valley. Clearly, there are vectors pointing to (or from) this valley and they can be extracted by applying a differential operator.

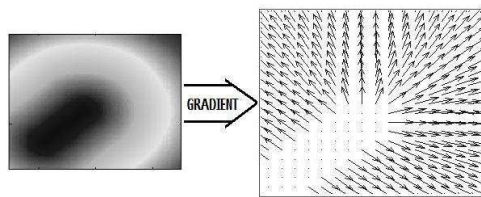


Figure 5: An image after application of distance transform, this distance map can be transformed by a gradient operator in order to get a vectorial map (below).

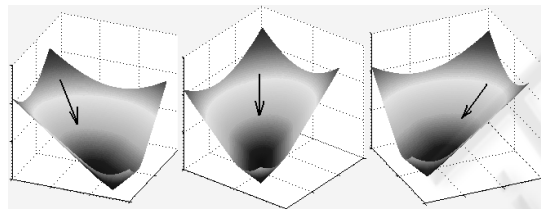


Figure 6: Three views of a distance map. The map looks like a geographical valley where the feature of interest lying on its bottom.

#### 4.4 Automatic Initialization

In its first flash of existence an electrical discharge usually resembles a straight line linking two points, similarly its projections look like low curvature curves. At this moment the discharge can be seen as an 3D vector whose extremities are points  $A$  and  $B$ . This vector can be easily recovered by triangulation of two pairs of points projected at the pair of images taken. Such points corresponds to  $A_1$  and  $A_2$ ,  $B_1$  and  $B_2$  in Fig. 7, these are used for triangulation (Trucco and Verri, 1998) in order to get  $A$  and  $B$ .

The 3D vector  $V$  is defined by  $V = B - A$ , and the set of points  $C$  that are generated by this vector are determined by  $p = A + cV$ , where  $c \in \mathbb{R}$  and  $0 \leq c < 1$ . Geometrically, the set  $C$  corresponds to the reconstruction of the electrical discharge in 3D at its initial instants of existence. These 3D points are approximated by a third order B-spline ( $\mathcal{B}_0$ ) the first spatial representation of the 3D-snake.

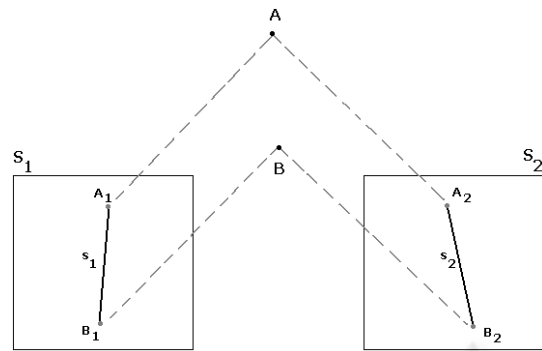


Figure 7:  $A$  can be determined by triangulation (Trucco and Verri, 1998) based on  $A_1$  and  $A_2$  its projections, similarly,  $B$  can be found by triangulation by  $B_1$  and  $B_2$ . It is possible to triangulate  $A_1$  and  $A_2$  to obtain  $A$ , as well as  $B_1$  and  $B_2$  to obtain  $B$ .  $A$  and  $B$  are extremities of the electrical discharge in 3D.

#### 4.5 Deformation

The 3D-snake, represented by a B-spline, should deform itself according of the minimization of its total energy functional described in Eq. 1. The snake converges to a stable configuration when a minimum of energy has been obtained which means that the deformation should stop because an equilibrium of the internal and external forces has been reached. The goal here is a tracking operation, so the snake needs to find the equilibrium for each pair of vectorial map available.

Now, consider the set of  $i$  pairs of vectorial maps, where  $m_i^j$  represents a map in  $i$ th time and associated to the  $j$ th camera:  $\mathcal{M} = \{(m_0^1, m_0^2); (m_1^1, m_1^2); \dots; (m_{i-1}^1, m_{i-1}^2)\}$ . Also, consider  $\mathcal{B}_0$  as the 3D-snake obtained for the first pair  $(m_0^1, m_0^2)$ . In order to get the next spatial configurations of the 3D-snake, it is necessary to minimize the functional in Eq. (1) under the influence of the next pair of maps. Following such path, the configuration represented by  $\mathcal{B}_1$  results from the evolution of  $\mathcal{B}_0$  adjusted to the pair  $(m_1^1, m_1^2)$ ,  $\mathcal{B}_2$  results from the evolution of  $\mathcal{B}_1$  adjusted to  $(m_2^1, m_2^2)$  and so on, up to the  $(i - 1)$ th pair of maps when all of the possible spatial configurations have been taken in three-dimensional space.

### 5 RESULTS

The actual lengths of the helixes versus the ones calculated by 3D-snake are shown in Fig. 8. Also, for each helix the average of its curvature was calculated and is exhibited in Fig. 9 and the deviation is shown in Fig. 10.

The deviation rises according to the rising of the curvature of the helixes. On the other hand, the 3D-snake provides a good estimate for the length of the electrical discharge, as seen in Fig. 8 the measurements made through the 3D-snake model follow the profile determined by the actual measurements.

The model works well for medium and low curvatures which represents an improvement in comparison with methods found in the literature .

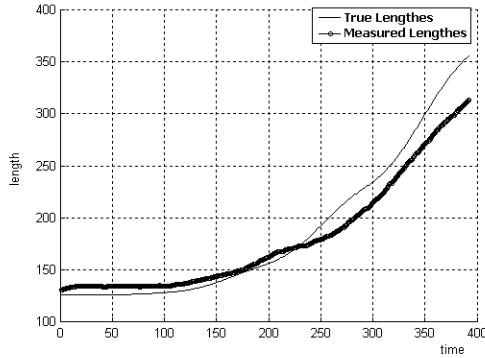


Figure 8: Real lengths of the helixes versus lengths calculated by 3D-snake model.

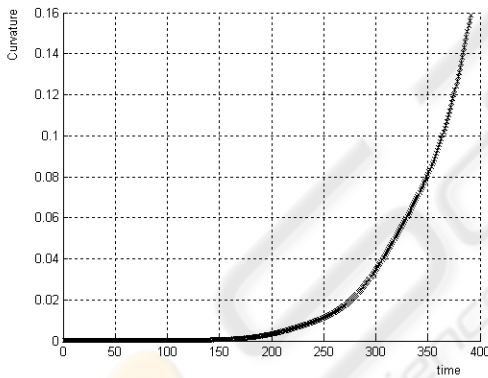


Figure 9: Real curvature for each helix created by Eq.(19).

### 5.1 Testing the Proposal with Real Discharges

Since the approach was validated with synthetic curves, it will be applied to real images. A pair of digital cameras *Sony*<sup>®</sup> DSC-P200, at 30 fps, was used to capture the discharge images produced in the apparatus called Plasma Ball driven by capacitive effect (Fig. 11). The cameras were calibrated by a chess pattern, according Trucco's method (Trucco and Verri, 1998). The Plasma Ball is a very safe and cheap way to produce electrical discharges, it is basically a glass

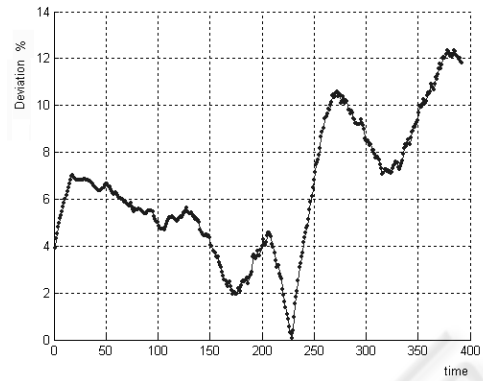


Figure 10: Average deviation for each measured on 3D-snake.

bulb filled with a special gas and a source of alternating high voltage (not as high as produced by a Tesla coil). When the glass bulb is touched, from the outside, a bright discharge is generated by the electrical field produced on that point. The arcs are produced by the high voltage and the physical effect called capacitive force, in regions inside the ampoule where the gas become more conductive, see Fig. 12.

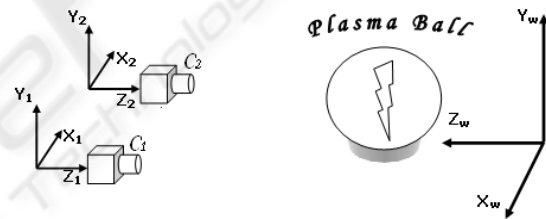


Figure 11: Acquisition system:  $C_1$  (*Sony*<sup>®</sup> P100) and  $C_2$  (*Sony*<sup>®</sup> P200) usual digital cameras. The plasma ball is the apparatus used for producing the electrical discharges.

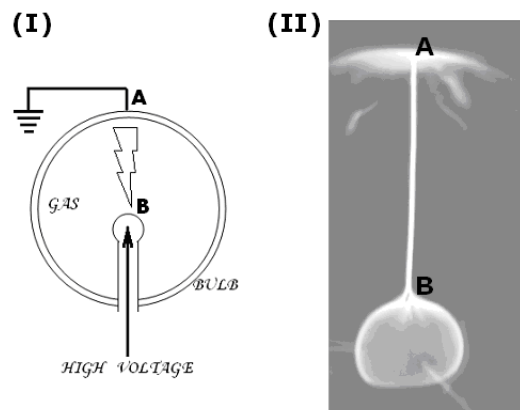


Figure 12: (I) Details of the Plasma Ball: distance  $AB$  is  $d_{AB} \approx (60 \pm 0.5)mm$ . (II) Electrical discharge produced.

A set of image pairs was captured followed by

the approach proposed to do the measurements of the discharge, based on the 3D-snake. As an example, was obtained for the discharge lengths:  $\approx (60.46 \pm 0.44)mm$ . The set of discharges presents very low curvature, so the distance  $d_{AB} \approx (60 \pm 0.5)mm$  shown in (Fig. 12) is a good result for the true length, allowing characterization of the electrical discharges, such as current density and other electrical parameters.

After these experiments the method will be applied to high voltage transmission lines.

## 6 CONCLUSIONS

This work described and validated an approach to be applied in modelling of electrical discharges captured in a sequence of stereo pairs. The approach was tested with an image database built by a consistent strategy and the cameras were based on the classical theoretical pinhole camera model.

The results obtained by 3D-snake in estimating the length of the curves are coherent with the real lengths. Since the cameras are calibrated it is also possible to determinate the real position of the electrical discharge during the time of the image acquisition, so the approach proposed here can work as a strategy for tracking. A new field of application for 3D active contours is opened, such as the tracking of electrical discharges captured in a pair of digital videos and the study of fast events.

Thus, in the near future this methodology will be applied in the studies of real electrical discharges where, certainly, will be found new constraints and more critical requirements to be evaluated.

## ACKNOWLEDGEMENTS

The authors thank the financial support received from FAPESP - The State of São Paulo Research, from CNPq - The National Council for Scientific and Technological Development and from CAPES - Coordination of Improvement of Higher Level Education Personnel. Special thanks to Mr. Marco Iacovacci.

## REFERENCES

Amarasinghe, D., Sonnadara, U., Berg, M., and Cooray, V. (2007). Correlation between brightness and channel currents of electrical discharges. *IEEE Transactions on Dielectrics and Electrical Insulation*, 14(5):1154–1160.

Amini, A. A., Tehrani, S., and Weymouth, T. E. (1988). Using dynamic programming for minimizing the energy of active contours in the presence of hard constraints. In *Second International Conference in Computer Vision*, pages 95–93.

Blake, A. B. and Isard, M. (2000). *Active Contours*. Springer, 2nd edition. Available at URL: <http://research.microsoft.com/>

Canero, C. (2002). *3D Reconstruction of the Coronary Tree Using Biplane Snakes*. PhD thesis, Universitat Autònoma de Barcelona, Bellaterra.

Canero, C., Radeva, P., Toledo, R., Villanueva, J. J., and Mauri, J. (2000). 3d curve reconstruction by biplane snakes. In *Proceedings of the International Conference on Pattern Recognition (ICPR'00)*, volume 4, pages 4563–4566.

Ihlow, A. and Seiffert, U. (2005). Snakes revisited : Speeding up active, contours models using the fast fourier transform. In *Proceedings of the Eighth IASTED International Conference : Intelligent Systems and Control*, pages 416–420.

Kass, M., Witkin, A., and Terzopoulos, D. (1988). Snakes: Active contours models. *Second International Conference in Computer Vision*, 1(4):321–331.

MacAlpine, J. M. K., Qiu, D. H., and Li, Z. Y. (1999). An analysis of spark paths in air using 3-dimensional image processing. *IEEE Transactions on Dielectrics and Electrical Insulation*, 6(3):331–336.

Qiu, D. H. and MacAlpine, J. M. K. (2000). An incremental analysis of spark paths in air using 3-dimensional image processing. *IEEE Transactions on Dielectrics and Electrical Insulation*, 7(6):758–763.

Qiu, D. H., MacAlpine, J. M. K., and Li, Z. Y. (1999). An incremental 3-dimensional analysis of spark paths in air. In *Conference on Electrical Insulation and dielectric Phenomena*, volume 2, pages 646–649.

Rogers, D. F. and Adams, J. A. (1990). *Mathematical Elements for Computer Graphics*. Mc-Graw Hill.

Thevenaz, P. and Unser, M. (2008). Snakuscles. *IEEE Transactions on Image Processing*, 17(4):585–593.

Trucco, E. and Verri, A. (1998). *Introductory techniques for 3D Computer Vision*. Prentice Hall.

Williams, D. J. and Shah, M. (1992). A fast algorithm for active contours and curvature estimation. In *Proceedings of Computer Vision, Graphics, and Image Processing*, volume 55, pages 14–26.

Xu, C. and Prince, J. L. (1998). Snakes, shapes, and gradient vector flow. *IEEE Transactions on Image Processing*, 7(3):359–369.